Jurnal Teknik Mesin, Industri, Elektro dan Informatika
Volume 5, Nomor 2, Juni 2026
e-ISSN: 2963-7805; p-ISSN: 2963-8208, Hal. 337-351
DOI: https://doi.org/10.55606/jtmei.v5i2.6137
Tersedia: https://ejurnal.politeknikpratama.ac.id/index.php/jtmei

Numerical Assessment of a Modified Hypoplastic Model with Enhanced Stability in Finite Element Simulations

Sendy Fransiscus Tantono
Civil Engineering Department, Widya Karya Catholic University, Indonesia
**Corresponding Author:* sendytantono@widyakarya.ac.id

Abstract. This study presents a comprehensive numerical investigation of a modified stress integration scheme applied to a simple hypoplastic constitutive model originally proposed by Wu Wei (1992). The modification aims to improve numerical stability, enhance convergence behavior, and eliminate spurious inhomogeneous deformation that frequently occurs in finite element simulations using conventional hypoplastic formulations. A fully implicit stress update algorithm incorporating a stability-controlled interpolation parameter is developed and implemented within the finite element framework. The proposed approach is evaluated through a series of numerical simulations, including oedometer compression, plane strain compression, and footing penetration tests conducted using Abaqus software. The simulation results indicate that the modified algorithm significantly improves computational robustness by reducing numerical oscillations and suppressing artificial shear stress evolution during loading. Furthermore, the method ensures homogeneous deformation at the element level, resulting in more reliable and physically consistent predictions. A comparative assessment with the elastoplastic Drucker–Prager model demonstrates that the modified hypoplastic formulation provides a more realistic representation of stress evolution, volumetric behavior, and dilatancy characteristics in granular materials. Overall, the proposed framework offers a stable, efficient, and accurate approach for finite element modeling of hypoplastic materials and has strong potential for application in advanced geotechnical engineering analyses.

Keywords: Finite Element Method; Granular Materials; Hypoplasticity; Numerical Stability; Stress Integration.

1. INTRODUCTION

Hypoplasticity has emerged as a powerful constitutive framework for modeling granular materials without the need for yield surfaces or plastic potential functions. Despite its theoretical advantages, numerical implementation of hypoplastic models in finite element analysis initially suffers from instability issues. In particular, spurious inhomogeneous deformation may arise even in single-element simulations. These numerical artifacts are generally associated with the uncontrolled evolution of shear stress during incremental loading. The proposed approach is validated through numerical simulations of oedometer compression, plane strain compression, and footing penetration tests. Results are compared with both the original hypoplastic formulation and the classical Drucker–Prager model.

2. LITERATURE REVIEW

Hypoplastic Constitutive Equations

In the hypoplastic model, the stress increment equation is expressed in rate form as:

$$\overset{\circ}{\mathbf{T}}_{ij} = \mathbf{L}_{ijkl} : \mathbf{D}_{kl} + \mathbf{N}_{ij} \left\| \mathbf{D}_{kl} \right\| \quad \text{(i)}$$

with $\overset{\circ}{\mathbf{T}}$ the Jaumann stress rate and D strain rate. The colon : denotes inner product between two tensors and $\left\|\mathbf{D}\right\| = \sqrt{\mathbf{D}:\mathbf{D}}$. The Hypoplastic contitutive equation is decomposed

Received*: April 10, 2026;* Revised*: May, 15 2026;* Accepted*: June 12, 2026;* Available*: June 19, 2026*

into linear part, $\mathbf{L}_{\mathrm{ijkl}}:\mathbf{D}_{\mathrm{kl}}$ and nonlinear part, $\mathbf{N}_{\mathrm{ij}}\left\|\mathbf{D}_{kl}\right\|$ in strain rate tensor. This study specifically adopted hypoplastic contitutive equations proposed by Wu Wei (1992) as follows

$$\overset{\circ}{\mathbf{T}}_{\mathrm{ij}}=C_1(\mathrm{tr}\,\mathbf{T})\mathbf{J}_{\mathrm{ijkl}}\mathbf{D}_{\mathrm{kl}}+C_2\frac{(\mathbf{T}_{\mathrm{kl}}:\mathbf{D}_{\mathrm{kl}})}{\mathrm{tr}\,\mathbf{T}}\mathbf{T}_{\mathrm{ij}}+C_3\frac{\mathbf{T}_{\mathrm{ij}}\mathbf{T}_{\mathrm{ij}}}{\mathrm{tr}\,\mathbf{T}}\left\|\mathbf{D}_{\mathrm{kl}}\right\|+C_4\frac{\mathbf{T}^{\mathrm{d}}_{\mathrm{ij}}\mathbf{T}^{\mathrm{d}}_{\mathrm{ij}}}{\mathrm{tr}\,\mathbf{T}}\left\|\mathbf{D}_{\mathrm{kl}}\right\| \ldots\ldots\ldots\ldots\ldots\ldots\ldots\text{(ii)}$$

where C_i (i = 1,…,4) are dimensionless parameter, $\mathbf{J}_{\mathrm{ijkl}}$ is described by $\mathbf{J}_{\mathrm{ijkl}}=\delta_{ik}\delta_{jl}$. In Eq. 2 the deviatoric stress tensor is given by $\mathbf{T}^{\mathrm{d}}_{\mathrm{ij}}=\mathbf{T}_{\mathrm{ij}}-1/3*(\mathrm{tr}\,\mathbf{T})\mathbf{1}$.

Modified Stress Integration Scheme

Since the material behavior is rate independent a fictitious time scale can be introduced for a quasi-static loading process. A loading stress is divided into increments, which corresponds to a division of a prescribed time domain into time increments. Once the displacement increment is obtained, the stress can be updated by using the implicit integration formulation. The unknown stress at time t = n+1 can be determined as

$$\mathbf{T}_{\mathrm{t=n+1}}=\mathbf{T}_{\mathrm{t=n}}+\Delta\mathbf{T} \ldots\ldots\ldots\ldots\ldots\ldots\ldots\ldots\ldots\ldots \text{(iii)}$$

where $\Delta\mathbf{T}$ is the stress increment equation calculated from Eq. 2. In addition, the modification of stress increment $\Delta\mathbf{T}$ is shown in Eq. 6. Here, Taylor expansion is introduced in the linear and nonlinear part of Eq. 1 as

$$\mathbf{L}^{\mathrm{n+\theta}}_{\mathrm{ijkl}}=\mathbf{L}^{\mathrm{n}}_{\mathrm{ijkl}}+\theta\frac{\partial\mathbf{L}^{n}_{\mathrm{ijkl}}}{\partial\mathbf{T}_{\mathrm{ab}}}:\Delta\mathbf{T}_{\mathrm{ab}} \ldots\ldots\ldots\ldots\ldots\ldots\ldots\ldots \text{(iv)}$$

$$\mathbf{N}^{\mathrm{n+\theta}}_{\mathrm{ij}}=\mathbf{N}^{\mathrm{n}}_{\mathrm{ij}}+\theta\frac{\partial\mathbf{N}^{n}_{\mathrm{ij}}}{\partial\mathbf{T}_{\mathrm{ab}}}:\Delta\mathbf{T}_{\mathrm{ab}} \ldots\ldots\ldots\ldots\ldots\ldots\ldots\ldots \text{(v)}$$

where θ is interpolation parameter and for stability $\theta>0.5$. By taking $\theta>1.0$ and substituting Eqs. 4 & 5 into Eq. 1, stress increment $\Delta\mathbf{T}$ in Eq. 3 reads as

$$\Delta\mathbf{T}_{\mathrm{ab}}=\left[\mathbf{J}_{\mathrm{ijab}}-\left({}^{\mathrm{d}\mathbf{L}_{\mathrm{ijkl}}}\!\big/_{\mathrm{d}\mathbf{T}_{\mathrm{ab}}}\right):\mathbf{D}_{\mathrm{kl}}*\Delta\mathrm{t}-\left({}^{\mathrm{d}\mathbf{N}_{\mathrm{ij}}}\!\big/_{\mathrm{d}\mathbf{T}_{\mathrm{ab}}}\right)\left\|\mathbf{D}*\Delta\mathrm{t}\right\|\right]^{-1}*\left(\mathbf{L}_{\mathrm{ijkl}}:\mathbf{D}_{\mathrm{kl}}*\Delta\mathrm{t}+\mathbf{N}_{\mathrm{ij}}\left\|\mathbf{D}*\Delta\mathrm{t}\right\|\right). \text{(vi)}$$

with $\mathbf{J}_{\mathrm{ijkl}}=\delta_{ik}\delta_{jl}$ ……………………………………………………………..…..(vii)

The stiffness matrix K_{ij} can be described from implicit function, reads

$$\begin{aligned}\mathbf{F}\equiv&-\Delta\mathbf{T}_{\mathrm{ij}}+\mathbf{L}_{\mathrm{ijkl}}:\mathbf{D}_{\mathrm{kl}}*\Delta\mathrm{t}+\mathbf{N}_{\mathrm{ij}}\left\|\mathbf{D}\right\|*\Delta\mathrm{t}+\\&+\left(\left({}^{\mathrm{d}\mathbf{L}_{\mathrm{ijkl}}}\!\big/_{\mathrm{d}\mathbf{T}_{\mathrm{ab}}}\right):\mathbf{D}_{\mathrm{kl}}*\Delta\mathrm{t}\right):\Delta\mathbf{T}_{\mathrm{ab}}+\theta*\left(\left({}^{\mathrm{d}\mathbf{N}_{\mathrm{ij}}}\!\big/_{\mathrm{d}\mathbf{T}_{\mathrm{ab}}}\right)\left\|\mathbf{D}\right\|*\Delta\mathrm{t}\right):\Delta\mathbf{T}_{\mathrm{ab}}=\mathbf{0}\end{aligned} \ldots\ldots\ldots\ldots \text{(viii)}$$

and

$$\mathbf{K} = -\frac{\partial \mathbf{F} / \partial (\mathbf{D}_{kl} \Delta t)}{\partial \mathbf{F} / \partial (\Delta \mathbf{T}_{ab})} \quad \text{(ix)}$$

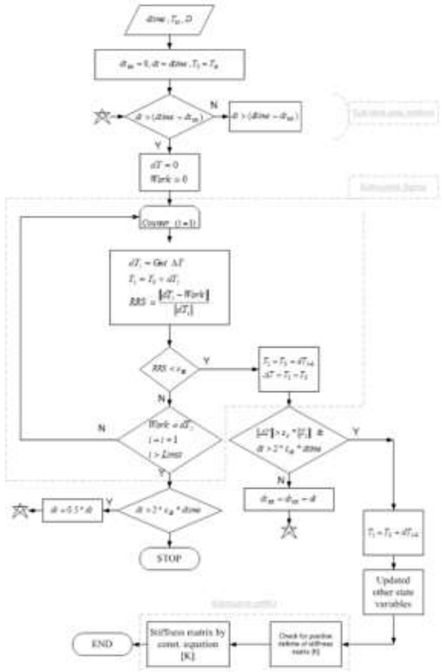

Figure 1. Flow Chart of the Time Integration Scheme.

For the nonsymmetric matrix, the stable condition of critical state could be maintained by checking the positiveness of all eigen-values of matrix $K_{new} = 0.5*(K + K^T)$, not of matrix K (de Borst, 1986). In order to check the positiveness of eigen-values, Bromwich (1906) stated that every eigen-value of nonsymmetric matrix satisfies $\hat{\lambda}_1 \leq \mathrm{Re}\ \lambda \leq \hat{\lambda}_n$. where $\hat{\lambda}_1$ and $\hat{\lambda}_n$ are the smallest and largest eigen-values, respectively. Therefore by only checking the positiveness of smallest eigen-value of K_{new}, the stability of critical state is obtained (Bazant & Cedolin, 2003). The detail algorithm is drawn in the flowchart shown in Fig.1.

Finite Element Simulations

In this finite element calculation by Abaqus ver.6.3, three tests were simulated, namely oedometric compression test, plane strain compression test, and penetration of footing into sand specimen. For oedometric test and plane strain compression test, the simulations are carried out by using a single element and discrete structure. In all simulations, a four nodes linear element is used. The comparison results between using original algorithm and modified algorithm described above are shown. Incase of the simulation of footing penetration, only the result by modified algorithm is shown and compared with those simulation by using elasto-plastic Drucker Prager model.

In these simulations, a nonlinear geometry analysis is applied, as consequences, local instabilities problem might occur due to local transfer of energy between elements. This can be solved by introducing artificial mass matrix with damping factors into general nonlinear equilibrium equation, $P_{ex} - P_{in} - c * M * v = 0$, where P_{ex} and P_{in} are external and internal force, M, v, and c are artificial mass matrix calculated with unity density, nodal velocity and damping factor, respectively. It is worth to note that in Abaqus program, this artifical damping factor can be applied by using stabilize option. The material constants of dense and loose Karlsruhe sand used in this simulation are summarized in Table 1 (Wu & Bauer, 1994):

Table 1. Material Constant of dense and loose Karlsruhe sand.

Karlsruhe sand	C_1	C_2	C_3	C_4
Dense	-101.2	-962.1	-877.3	1229.2
Loose	-69.4	-673.1	-655.9	699.6

Modeling Oedometric test

Oedometric test is simulated with the dimension of 4 x 4 cm^2. Fig 2 shows boundary condition used in the oedometric test of single element. The procedure is described as the following: equilibrium of initial isotropic compression of 100 kPa is applied, downward vertical displacement of -0.2 cm is prescribed at top node of the specimen, unloading the vertical displacement up to -0.05 cm measured from the initial position.

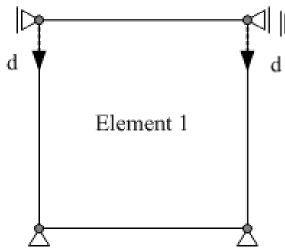

Figure 2. Simulation of Oedometric Test.

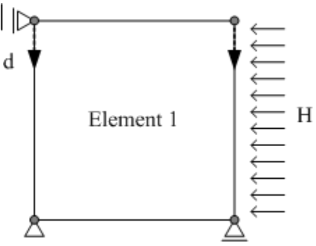

Figure 3. Simulation of Plane Strain Compression Test.

Modeling Plane Strain Compression test

Here, plane strain compression test is simulated as single element and discrete elements. The simulation of single element is conducted by using the same element size as that used in oedometric compression test while 4 x 8 cm^2 specimen is simulated by using 8 x 16 discrete elements. The procedure of loading is similar to that of for oedometric compression; after applying initial isotropic stress of 100 kPa, downward vertical displacement of 0.0036 m is prescribed on top of specimen with single element and that of vertical displacement of 2 cm is used for discrete element.

During the application of this displacement loading the lateral pressure H of 100 kPa is constantly applied on the right side of element. The boundary conditions used in plane strain compression test are shown in Fig 3.

Modeling Footing Penetration into sand

A 400 x 100 cm^2 box of soil specimen is also modeled by 48 x 40 four nodes linear elements while the footing is illustrated as a prescribed vertical displacement of 21.75 cm applied along 40 cm at the middle of soil box. The initial gravity loading of $2.0\,t/m^3$ is used before the footing penetrates the soil box and a vertical pressure of 1 kPa is applied on top surface of soil box. Since the footing is placed in the middle of soil box the problem may be considered in symmetry condition. It is worth to note that the smaller element size is used near the footing corner and the further the distance from footing the larger element size which is used, as shown in Fig. 4. In this simulation, the interface between footing and soil is assumed to be very rough so that no relative displacement is allowed between sand particle and footing surface. Here, two constitutive models are used and compared, namely hypoplastic model with modified algorithm described earlier and elasto-plastic Drucker Prager model. Parameter constants used in hypoplastic model is the same that used in oedometric and plane strain compression simulation while those used in elasto-plastic Drucker Prager model are chosen by fitting the results of the simulation of plane strain compression test done by hypoplastic model with modified algorithm (Figs. 24-25). The parameter constants resulted from curve-fitting are as follows.

Tabel 2. Modeling Footing.

Elastic mod. (kPa)	**Poisson ratio**	**Friction angle (deg.)**	**Dilation angle (deg.)**	$\tau\ at\ \sigma_N = 0$ **(kPa)**	K_{ratio}
3.036E+4	0.328	30	10	120	1.0

with K_{ratio} is a constant related to the shape of yield surface at the deviatoric plane; K=1.0 is circle.

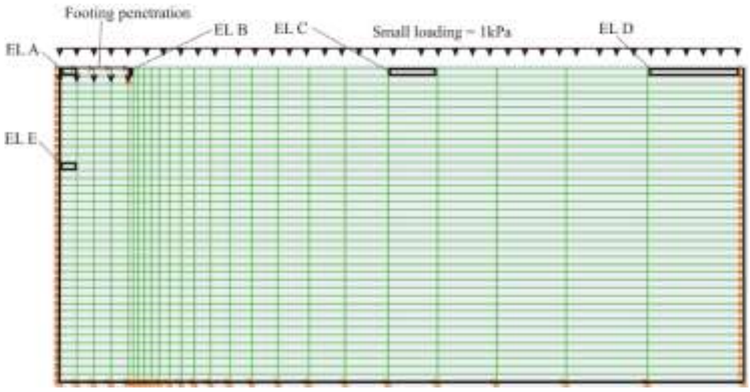

Figure 4. Illustration of Footing Penetration Into Sand Specimen.

3. RESULTS AND DISCUSSIONS

Oedometric test

Results of the simulation of oedometric test using single element are shown in Figs 5-7. In particular, Figs 5(a) & (b) show the normalized vertical (S_{22}/S_{11}) and shear stress (S_{12}/S_{11}) of dense and loose sand due to loading of -0.2 cm and unloading up to -0.05 cm. The value of normalized shear stress is very small ($< 10^{-17}$), which means that only homogeneous deformation occurs. However, a problem occurred when large loading - unloading of vertical displacement of -0.8 cm and 0.8 cm is applied on top of specimen. The calculation of original model failed before unloading step started. This might be happened because the element is no longer homogeneous where the shear stress increases very fast. By using a modification which is described in Section 2, a more stable result can be obtained, in the sense that the deformation of single element test is in homogeneous shape.

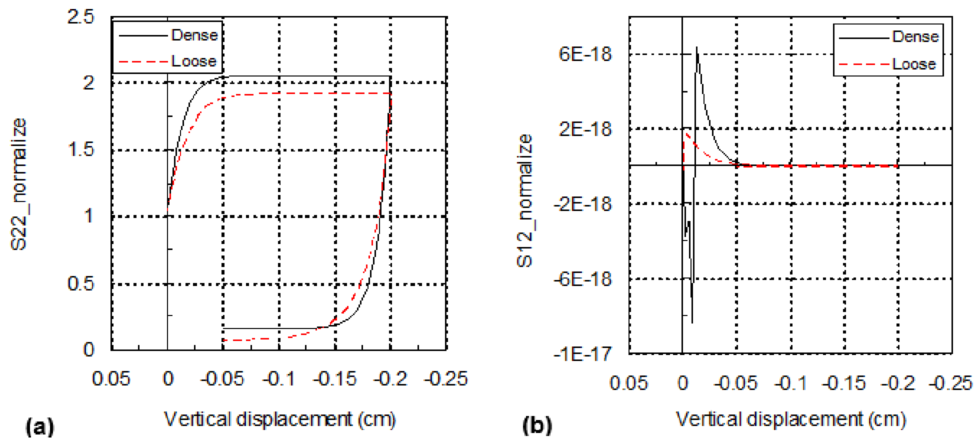

Figure 5. Evolution of normalized (a) vertical stress, (b) shear stress for loading / unloading.

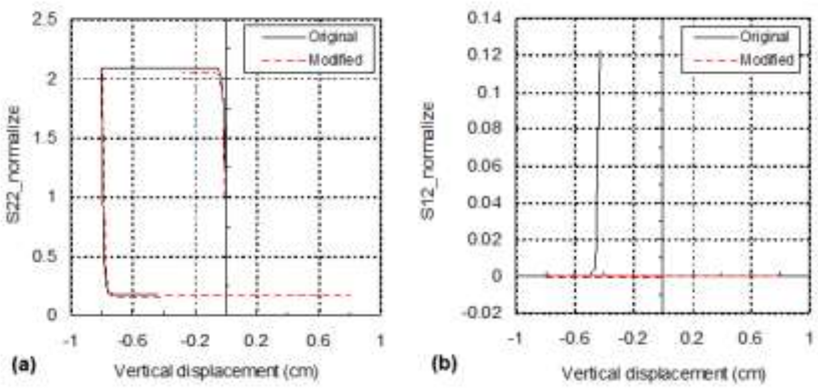

Figure 6. Comparison between original model and modified model during large.

Loading/unloading: evolution of normalized (a) vertical stress, (b) shear stress. The comparison results between applying original and modified algorithm version on the oedometric simulation with loading - unloading vertical displacement of -0.8 - 0.8 cm are shown in Fig 6(a) & (b) for normalized vertical stress and normalized shear stress, respectively. The evolution of coefficient earth pressures K_0 of dense sand and loose sand is shown in Fig 7. In loading condition, they are 0.487 and 0.521 for dense and loose sand. Nonlinear behavior of K_0 is clearly observed when un-loading condition is applied.

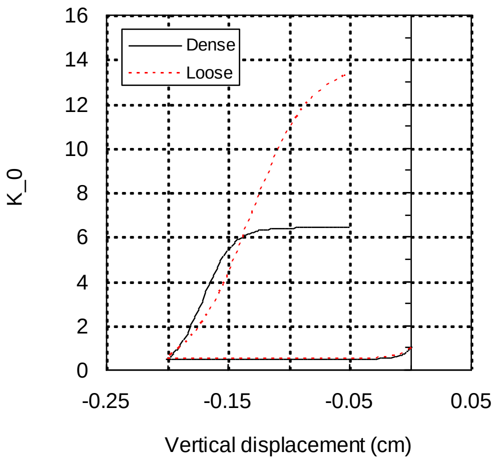

Figure 7. Evolution of coeficient of earth pressure at rest K_0 under loading-unloading.

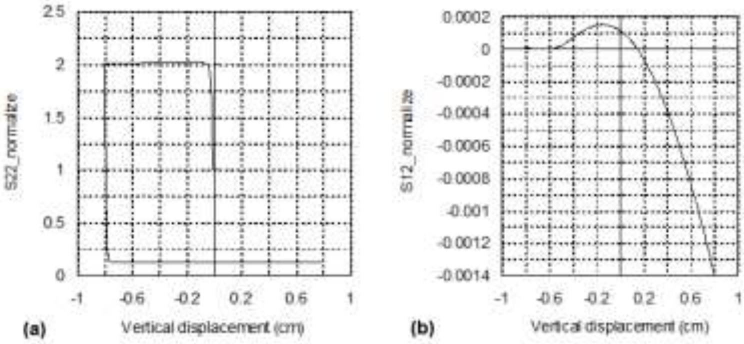

Figure 8. Evolution of (a) normalized vertical stress, (b) normalized shear stress.

In addition to single element, the behavior of discrete element (4 x 4 elements) of 4 x 4 cm^2 under loading and unloading condition is also investigated. The procedure is the same as that is used for single element. The results show that the behavior of normalized vertical stress is the same that of single element as shown in Fig. 8(a). Fig. 8(b) shows the evolution of shear stress during loading and unloading. It is clear that during loading no shear stress develops , while after certain unloading of vertical displacement the shear stress starts to develop to small values compared to that of horizontal stress.

Plane Strain Compression test

In the single element test, the original model seems to work well for dense and loose specimens. The dilatancy behavior of dense sand, as well as compaction behavior of loose sand can be smoothly modeled as shown in Fig 9. The stress ratio of dense sand is stiffer and higher than that of loose sand (Fig. 10). However, similar to the inhomogeneity problem faced in the simulation of oedometric compression, the original model shows anomaly behavior when loading of vertical displacement higher than 0.0036 cm is applied, as shown in Fig 11. It can be observed that the evolution of horizontal displacement of Node1 and Node2 is slightly different. This inhomogeneity is clearly shown in the evolution of normalized shear stress S_{12}/S_{11}, volumetric strain and stress ratio S_{22}/S_{11} (Figs. 12-14). In particular, the normalized shear stress behavior (Fig. 12) suddenly increases at about vertical strain of -0.09 while a sudden drawdown of stress ratio (Fig. 14) is also observed at about the same vertical strain.

This inhommogeneity cannot be true since it is occurred in the single element test. Therefore, a modified algorithm described in Section 2 is needed. The results after using modified algorithm are shown in Figs. 15-18. Homogeneous deformation can be directly observed from the deform shape and evolution of normalized shear stress, as shown in Figs. 15 & 16. The normalized shear stress fluctuates in only very small values. The dilatancy behavior, as well as the stress ratio evolution of dense specimen under loading-unloading-reloading can also be smoothly captured, as shown in Figs 17 & 18.

In addition to the simulation of single element, the plane strain compression test is also simulated by using discrete elements, applying both types of stress update algorithms. By using modified algorithm, the calculation result shows inhomogeneity of the deformation shape after vertical displacement of 2 cm (Fig. 19). The corresponding evolution of normalized shear stress, volumetric strain and stress ratio at the middle element are shown in Fig. 20, Fig. 21, and Fig. 22, respectively. Here, the effect of inhomogeneity deformation is clearly shown by sudden decreased of stress ratio (Fig. 22). Comparing the original and modified algorithm, the initial compression can be smoothly captured by both algorithms; however, the dilatancy behavior of specimen cannot be shown smoothly by original one. The unsuccessful calculation due to convergence problem is shown after certain vertical displacement (Figs. 23 (a) & (b)).

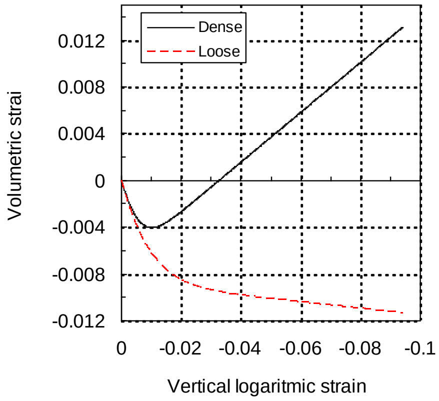

Figure 9. Evolution of volumetric strain.

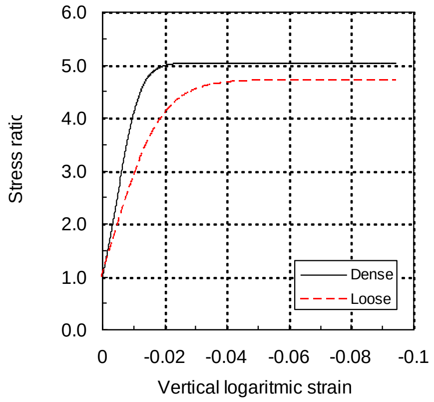

Figure 10. Evolution of stress ratio.

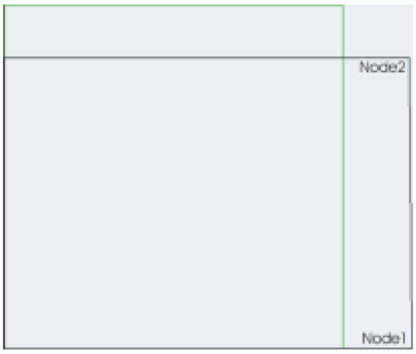

Figure 11. Deformed shape (original scheme).

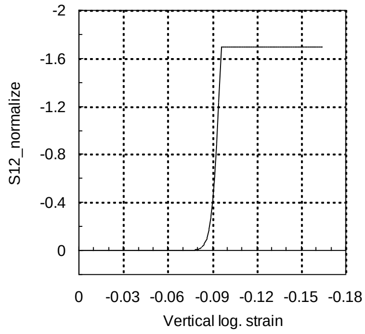

Figure 12. Evolution of normalized shear stress.

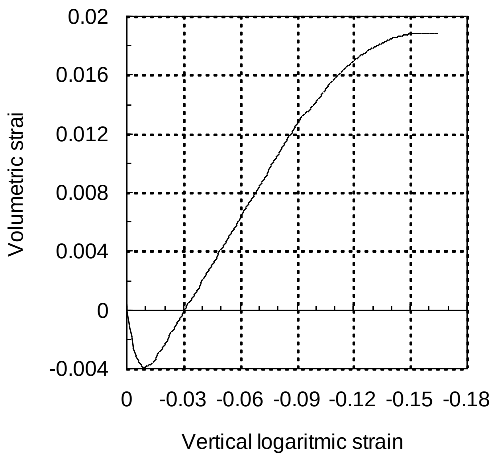

Figure 13. Evolution of volumetric strain.

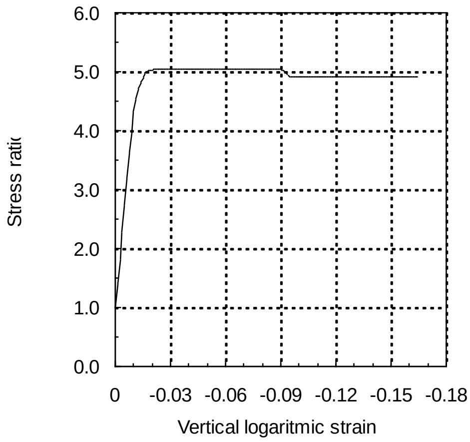

Figure 14. Evolution of stress ratio.

Figure 15. Deformed shaped (modified).

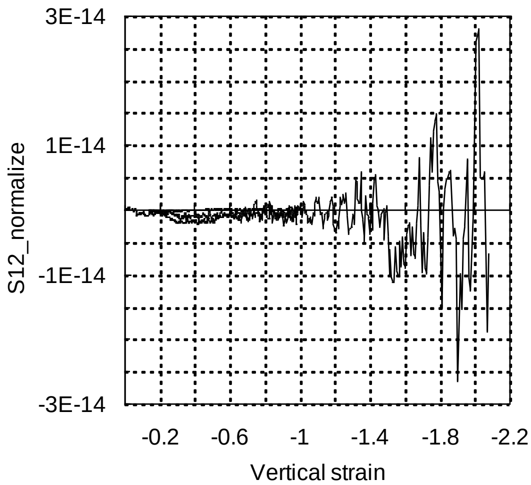

Figure 16. Evolution of normalized shear stress.

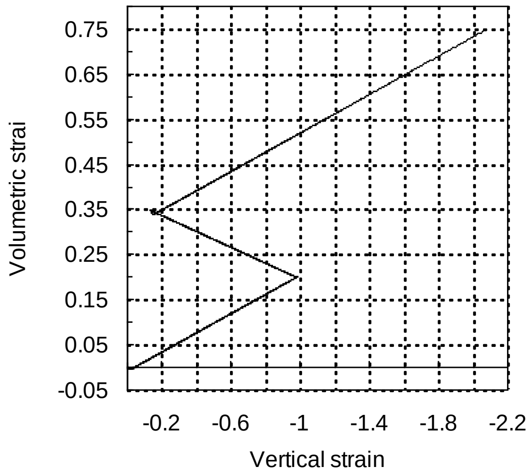

Figure 17. Evolution of volumetric strain.

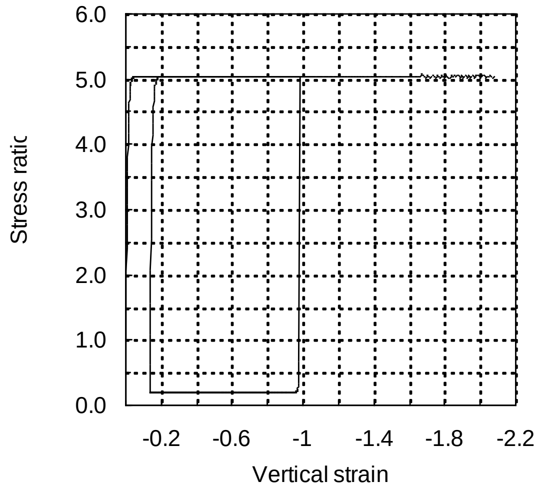

Figure 18. Evolution of stress ratio.

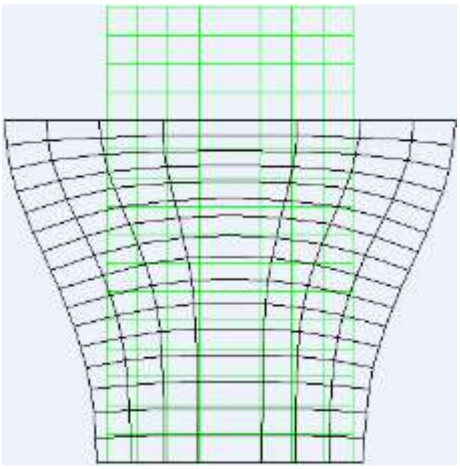

Figure 19. Deform shape (Modified).

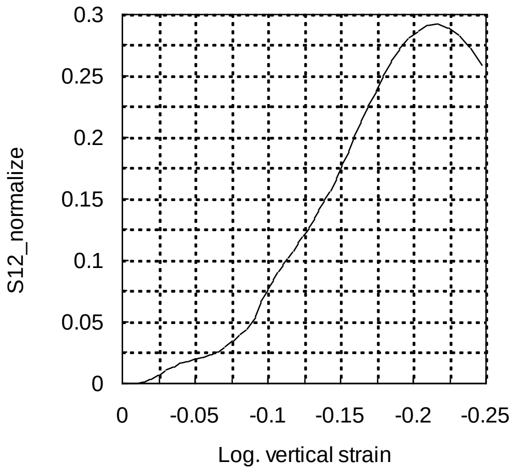

Figure 20. Evolution of normalized shear stress.

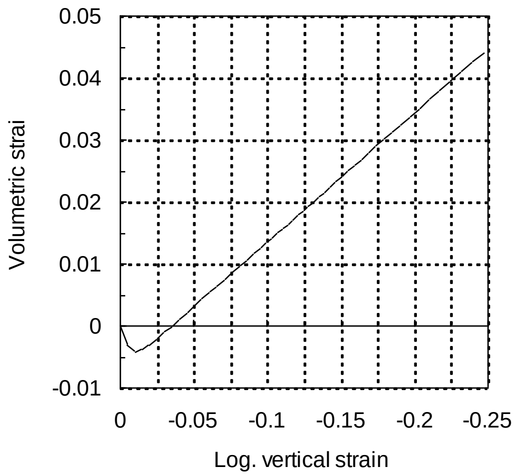

Figure 21. Evolution of volumetric strain.

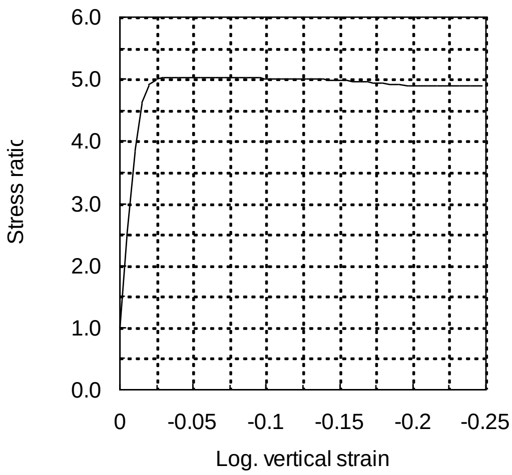

Figure 22. Evolution of stress ratio.

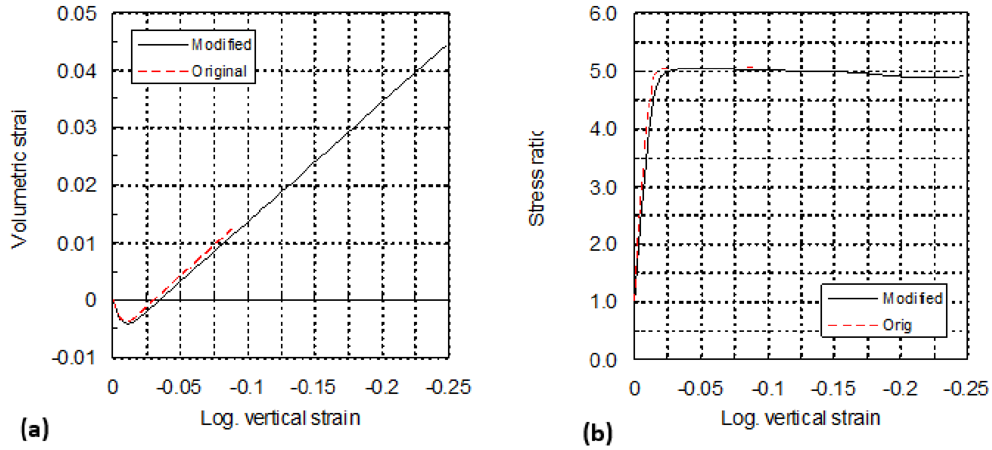

Figure 23. Comparison between original and modified algorithm for (a) Volumetric strain (b) Stress ratio.

Footing Penetration into Sand

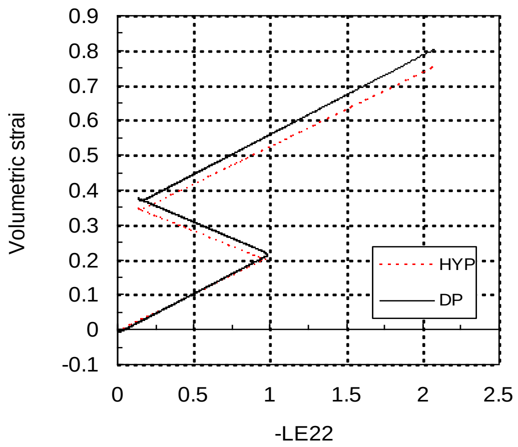

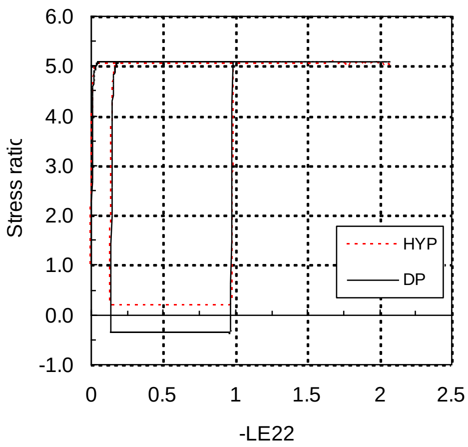

Figure 24. Evolution of volumetric strain. **Figure 25.** Evolution of Stress ratio.

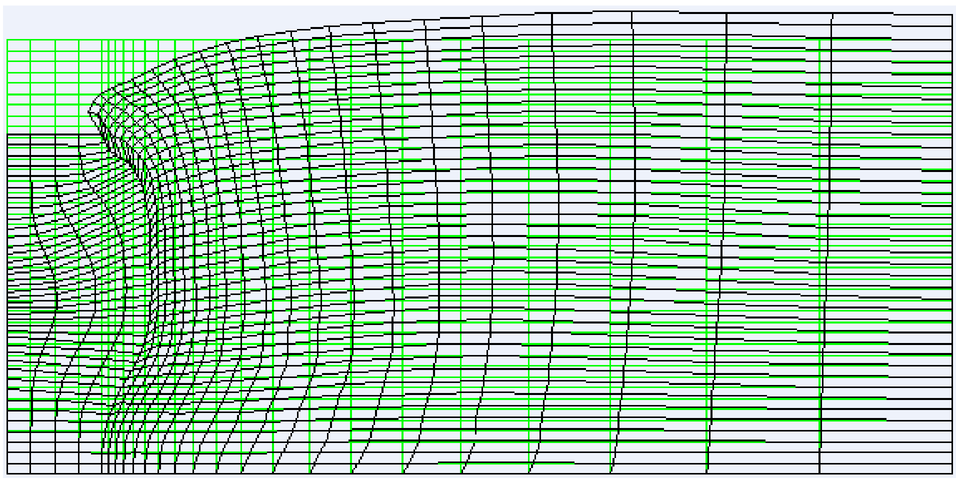

Figure 26. Deformed shape of sand specimen due to footing penetration – hypoplastic.

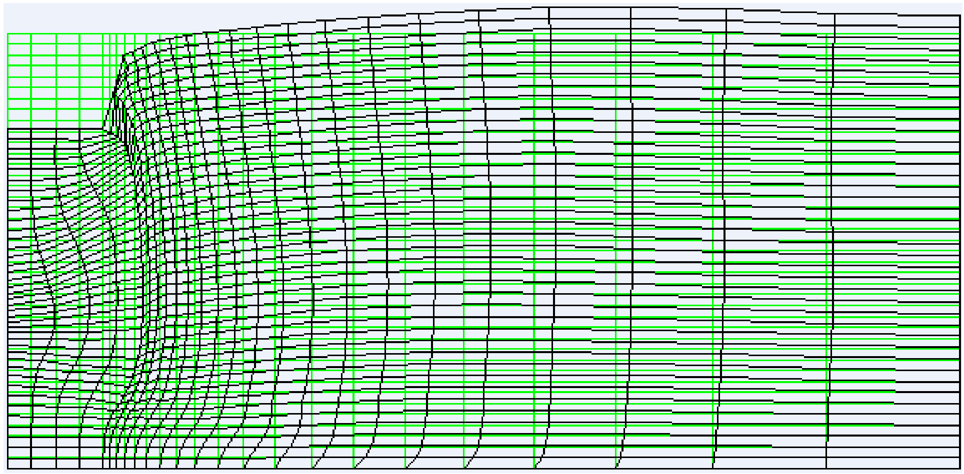

Figure 27. Deformed shape of sand specimen due to footing penetration – Drucker Prager.

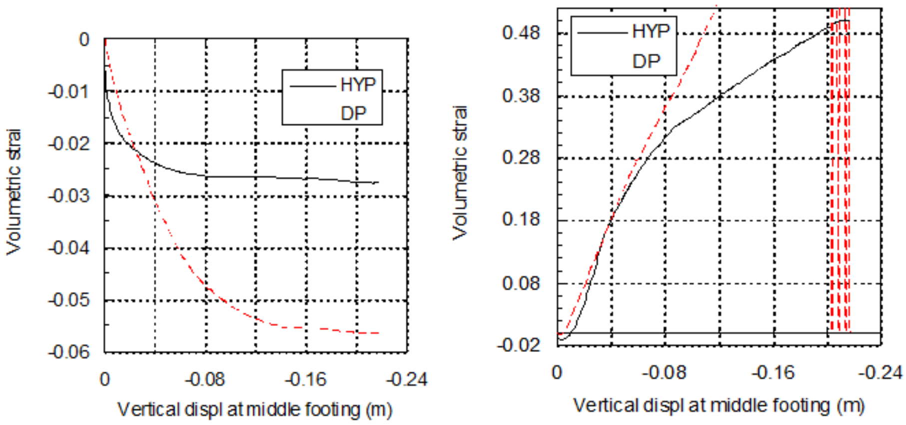

Figure 28. Comparison between hypoplastic model and elasto-plastic Drucker Prager model for Volumetric behavior of element (a) below, (b) at the corner of the footing.

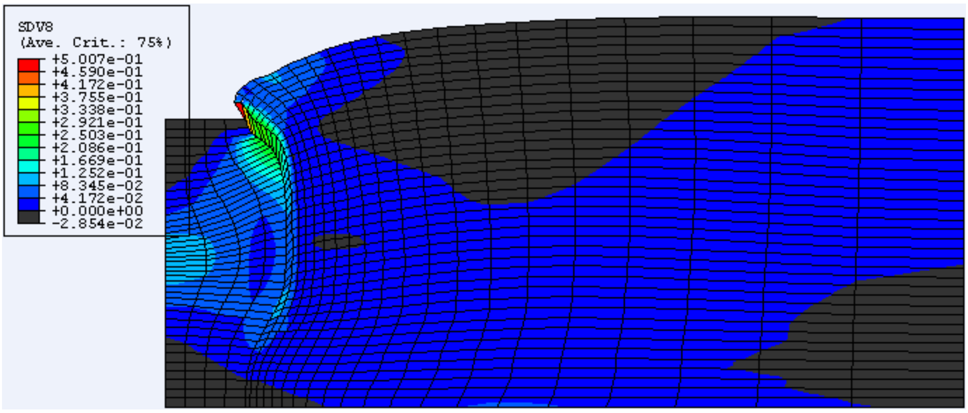

Figure 29. Volumetric behavior of sand around footing after penetration of 21.75 cm.

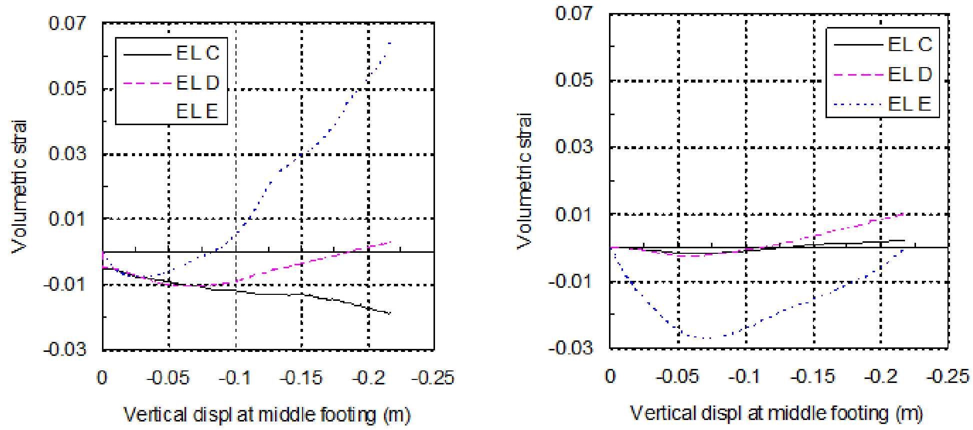

Figure 30. Evolution of volumetric strain at elements El. C, El. D, and El. E by using (a) hypoplastic model, (b) Elasto-plastic Drucker Prager model.

The results of the simulation show that in both models heaving of top surface soil specimen can be observed at the certain distance from the corner of the footing (Figs. 26 & 27). For the element EL A, Drucker Prager model give higher degree of compression, approximately twice of that by hypoplastic model (Fig. 28(a)) while the dilatancy behavior of the element at element EL B can be captured by hypoplastic model and the degree of dilatancy is only slightly different compared to that of by Drucker Prager model (Fig. 28 (b)). Here, the evolution of dilatancy behavior by Drucker Prager goes to the very high value. It should be noted that the oscillation behavior shown by Drucker Prager model (Fig. 28(b)) is due to the distortion of the element (see Fig. 27). Fig. 30 shows the volumetric behavior of the soil around the footing after penetration of 21.75 cm when the hypoplastic model is used. Here, the black color shows compression behavior (sign: negative). It shows that this contour of dilatancy behavior have a similar tendency as those shown by Prandtl mechanism. Detail dilatancy/compression behavior of element EL C, D, and E are shown in Fig. 30(a). It is also observed that the dilatancy behavior by elasto-plastic Drucker Prager model is not too pronounced compared to hypoplastic model, as shown in Fig. 30(b).

4. CONCLUSIONS

The simulations of oedometric compression, plane strain compression test, and penetration of footing into sand specimen are conducted by using hypoplastic model by Wu Wei (1992). The modification of stress update algorithm is introduced and used in those simulations. The inclusion of this modified algorithm shows an advantage in the sense of convergence especially for oedometric compression and plane strain compression tests. For the single element test, the simulation of oedometric and plane strain compression test using modified version can show homogeneous deformation for arbitrary loading/unloading condition. Homogeneous deformation is also shown when oedometric compression is simulated by using discrete structure while the inhomogeneous deformation is observed in plane strain compression test. This inhomogeneity is due to the material behavior and not due to geometrically reason. The penetration of footing foundation into sand specimen is simulated by using hypoplastic model with modified algorithm and elasto-plastic Drucker Prager model. Both models can capture a tendency of heaving at the certain distance from footing corner. The elasto-plastic Drucker Prager model shows slightly different degree of dilatancy angle at the element closed to the corner of footing. For the element below footing, the elastic-plastic Drucker Prager model shows twice higher degree of compression than that of hypoplastic model. The hypoplastic model can produce similar dilatancy behavior of the soil around the footing to those shown in Prandtl mechanism.

REFERENCES

Bazant, Z. P., & Cedolin, L. (2003). *Stability of structures: Elastic, inelastic, fracture and damage theories*. Dover Publications.

de Borst, R. (1986). *Non-linear analysis of frictional materials* (Doctoral dissertation, Delft University of Technology).

de Souza Neto, E. A., Perić, D., & Owen, D. R. J. (2011). *Computational methods for plasticity: Theory and applications*. Wiley.

Gudehus, G. (1996). A comprehensive constitutive equation for granular materials. *Soils and Foundations, 36*(1), 1–12. https://doi.org/10.3208/sandf.36.1

Kolymbas, D. (1991). An outline of hypoplasticity. *Archive of Applied Mechanics, 61*(3), 143–151. https://doi.org/10.1007/BF00788048

Kolymbas, D. (2000). *Introduction to hypoplasticity*. Balkema. https://doi.org/10.1201/9781482283785

Kolymbas, D., & Wu, W. (1993). Introduction to hypoplasticity. In D. Kolymbas (Ed.), *Modern approaches to plasticity* (pp. 213–223). Elsevier. https://doi.org/10.1016/B978-0-444-89970-5.50015-7

Li, X. S., & Dafalias, Y. F. (2000). Dilatancy of cohesionless soils. *Géotechnique, 50*(4), 449–460. https://doi.org/10.1680/geot.2000.50.4.449

Mašín, D., & Herle, I. (2022). Advanced constitutive modelling for granular soils. *International Journal for Numerical and Analytical Methods in Geomechanics, 46*(3), 455–479.

Niemunis, A. (1993). Hypoplasticity vs elastoplasticity. In D. Kolymbas (Ed.), *Modern approaches to plasticity* (pp. 277–307). Elsevier. https://doi.org/10.1016/B978-0-444-89970-5.50019-4

Niemunis, A. (2020). Extended hypoplastic models for granular materials. *Acta Geotechnica, 15*(5), 1201–1220.

Niemunis, A., & Herle, I. (1997). Hypoplastic model for cohesionless soils with elastic strain range. *Mechanics of Cohesive-Frictional Materials, 2*(4), 279–299. https://doi.org/10.1002/(SICI)1099-1484(199710)2:4<279::AID-CFM29>3.0.CO;2-8

Von Wolffersdorff, P.-A. (1996). A hypoplastic relation for granular materials with a predefined limit state surface. *Mechanics of Cohesive-Frictional Materials, 1*(3), 251–271. https://doi.org/10.1002/(SICI)1099-1484(199607)1:3<251::AID-CFM13>3.0.CO;2-3

Wood, D. M. (1990). *Soil behaviour and critical state soil mechanics*. Cambridge University Press. https://doi.org/10.1017/CBO9781139878272

Wu, W., & Bauer, E. (1994). A simple hypoplastic constitutive model for sand. *International Journal for Numerical and Analytical Methods in Geomechanics, 18*(12), 833–862. https://doi.org/10.1002/nag.1610181203